npj | 2D Materials and Applications

www.nature.com/npj2dmaterials

ARTICLE OPEN

Thickness dependent electronic properties of Pt dichalcogenides

Rovi Angelo B. Villaos[1], Christian P. Crisostomo[1], Zhi-Quan Huang[1], Shin-Ming Huang[1], Allan Abraham B. Padama[2], Marvin A. Albao[2], Hsin Lin[3] and Feng-Chuan Chuang[1]

Platinum-based transition metal dichalcogenides have been gaining renewed interest because of the development of a new method to synthesize thin film structures. Here, using first-principles calculation, we explore the electronic properties of PtX_2 (X = S, Se, and Te) with respect to film thickness. For bulk and layered structures (1 to 10 layers), octahedral 1T is the most stable. Surprisingly, we also find that the 3R structure has comparable stability relative to the 1T, implying possible synthesis of 3R. For a bulk 1T structure, PtS_2 is semiconducting with an indirect band gap of 0.25 eV, while $PtSe_2$ and $PtTe_2$ are both semi-metallic. Still, all their corresponding monolayers exhibit an indirect semiconducting phase with band gaps of 1.68, 1.18, and 0.40 eV for PtS_2, $PtSe_2$, and $PtTe_2$, respectively. For the band properties, we observe that all these materials manifest decreasing/closing of indirect band gap with increasing thickness, a consequence of quantum confinement and interlayer interaction. Moreover, we discover that controlling the thickness and applying strain can manipulate van Hove singularity resulting to high density of states at the maximum valence band. Our results exhibit the sensitivity and tunability of electronic properties of PtX_2, paving a new path for future potential applications.

npj 2D Materials and Applications (2019)3:2 ; https://doi.org/10.1038/s41699-018-0085-z

INTRODUCTION

Transition metal dichalcogenides (TMDs) are very old materials, among which is molybdenite (MoS_2), with the earliest sample dating back to more than 2.9 billion years ago.[1] Layered TMDs generally have the formula MX_2, where M corresponds to a transition metal, usually belonging to group IV-VII, and is sandwiched by X atoms which correspond to chalcogens, e.g., S, Se, and Te. The common structures of TMDs can either be trigonal prismatic or octahedral, which can be stacked into different polymorphs known as 1T, 2H, and 3R.[2] Studies regarding TMDs have already been done as early as 1923.[3] By 1960–1980s, comprehensive studies about their single to few layered structures,[4,5] as well as optical, electrical, and structural properties, have already been explored,[6] but these works were mostly overlooked. However, the interest in TMDs was rekindled with the discovery and success of graphene[7] which revolutionized our current understanding of two-dimensional (2D) materials. With this, layered TMDs, due to their easiness to be exfoliated[4] with van der Waal forces between layers, has become one of the alternatives for graphene.[8] Moreover, recent studies showed that the electronic properties of TMDs can easily be engineered and tuned just by varying its thickness[9,10] or inducing strain[11–14] which present immense possibilities for applications in solid-state physics and technological advancement.

Experimental[2,15,16] and theoretical[2,9,17,18] studies confirmed that the electronic properties of Mo- and W-based TMDs can be manipulated by controlling the number of layers (or thickness). It was observed that decreasing the number of layers (L) from bulk to monolayer corresponds to increasing band gap. Additionally, a transition from indirect to direct band gap also occurs when decreasing the thickness from bulk to monolayer. These interesting properties make TMDs one of the forerunners in materials research, especially in 2D materials.

Experimental investigations[19–27] on Pt-based TMDs have been conducted and were found to exhibit better characteristics than the other well-studied TMDs. Recently, a new technique to synthesize few layers of $PtSe_2$ by "direct selenization" of Pt metal was developed. It was found that the synthesized 1T-$PtSe_2$ using the said method have potential applications for photocatalysis and valleytronics.[19] Furthermore, by using Raman characterization, it is possible to determine the thickness of few-layered 1T-$PtSe_2$ fabricated through "direct selenization" technique.[20] In one study,[23] it was observed that the electron mobility at room temperature of $PtSe_2$ is significantly higher than MoS_2 implying that it has potential applications in field-effect transistors. Other studies also showed that these specific TMDs have unique electronic properties that are suitable for a wide range of optoelectronic device applications[21,22] and hydrogen-evolution reaction.[24] Moreover, theoretical studies[27–35] regarding noble TMDs, specifically on PtX_2 and PdX_2, have been conducted. However, they are mostly either focused on the properties of few-layer structures, or on other specific TMD materials. Furthermore, to the best of our knowledge, no studies have been done regarding the possibility of another stable structure, and about the presence of van Hove singularity on Pt-based TMDs. Thus, a detailed analysis for these materials focusing on thickness dependence is still lacking.

In this paper, we probed the behavior of the electronic properties of Pt-based TMDs (PtX_2 where X = S, Se, and Te) using

[1]Department of Physics, National Sun Yat-Sen University, Kaohsiung, Taiwan; [2]Institute of Mathematical Sciences and Physics, College of Arts and Sciences, University of the Philippines Los Baños, College, Laguna, Philippines and [3]Institute of Physics, Academia Sinica, Taipei, Taiwan
Correspondence: F-C. Chuang (fchuang@mail.nsysu.edu.tw)
These authors contributed equally: Rovi Angelo B. Villaos, Christian P. Crisostomo, Zhi-Quan Huang

Received: 3 July 2018 Accepted: 20 December 2018
Published online: 16 January 2019

first-principles calculations. Here, we specifically focused on the thickness dependence of the band structures by varying the number of layers from monolayer up to 10L, as well as the band structures of bulk PtX_2. With regards to the bulk structure of PtX_2, we also probed other existing structures of TMDs (2H and 3R) in which we confirmed that 1T is indeed the most stable structure of $PtSe_2$. However, we found that 3R has comparable formation energy relative to 1T, which suggested that it was indeed possible to synthesize this 3R structure. Finally, we studied the evolution of the highest occupied state of PtS_2 with respect to thickness and strain where we found possible van Hove singularity (vHs).[36] Previous studies have shown that vHs near the Fermi level enhances material property such as superconductivity,[37–39] ferromagnetism,[40,41] and antiferromagnetism.[42] Our results show that PtX_2 TMDs have their own interesting features which provide an initial basis for possible future applications and advancement of these materials.

RESULTS

In this study, Fig. 1 shows the crystal structures of octahedral 1T and 3R as well as the corresponding first Brillouin Zone (BZ). For bulk 1T and 3R PtX_2, the optimized lattice parameters together with the calculated formation energy per formula unit (E_F) and system band gap (E_G) are shown in Table 1. Table 2, on the other hand, shows the calculated formation energy per formula unit (E_F) and band gap (E_G) of the layered structures of 1T and 3R PtX_2 from monolayer up to 10L. The calculated bulk band structures are shown in Fig. 2. For the layered structures, the bulk lattice constants (see Table 1) are used to construct the layered structures starting from monolayer up to 10L. Crystal structure relaxations were performed again before determining the formation energies and electronic properties. To understand the effect of the thickness to the electronic structures of layered PtX_2 TMDs, we explored the structural and electronic properties of PtX_2 with respect to the number of layers. The calculated electronic band structures of multilayer PtS_2, $PtSe_2$, and $PtTe_2$ are presented, respectively, in Figs. 3, 4, and 5. For the vHs, the energy contour plots are shown in Figs. 6 and 7.

DISCUSSION

As seen in Fig. 1, both 1T and 3R have octahedral coordination for each unit layer but differ in layer stacking, i.e., AA (Fig. 1b) and ABC (Fig. 1c), respectively. Based on the calculated formation energies shown in Table 1, 1T is the stable structure for bulk PtX_2, while 3R is a metastable phase. With regards to our proposed metastable 3R structure, we based our initial assumptions on the experimental study[20] in which the authors were able to find $PtSe_2$ structures that are not 1T. From this result, we examined known bulk structures of TMDs—1T, 2H, and 3R combined with octahedral and trigonal prismatic coordination, and we found that octahedral 1T is indeed the most stable for bulk PtX_2 structure. Surprisingly, we found that octahedral 3R has a comparable stability relative to 1T based on the E_F, indicating the possibility of synthesis. Also, we define for this study the system band gap which is the difference in energy between the conduction band minimum (CBM) and the valence band maximum (VBM). Using this definition, we further define a semimetal as a material with a negative band gap.

Here, we discuss the calculated properties of the bulk PtX_2 structures. We start with 1T-PtS_2, which is the only semiconductor among the three 1T bulk structures. Our calculated lattice constants and band gap (Table 1) are a = 3.591 Å, c = 4.877 Å, and E_G = 0.25 eV which is in good agreement with the experimental lattice parameters (a = 3.543 Å, c = 5.039 Å) and band gap

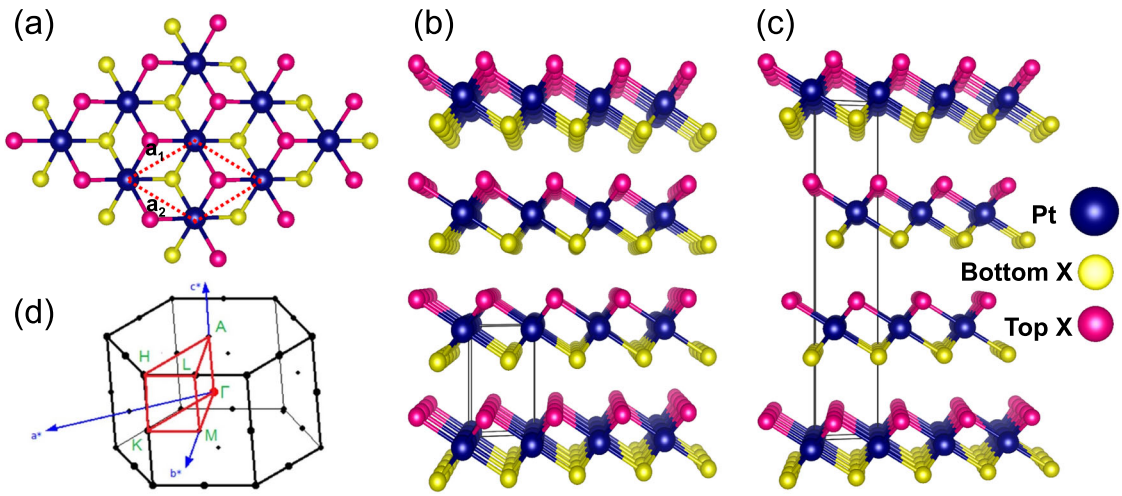

Fig. 1 **a** Top view of the optimized bulk 1T layered structure. Side views of **b** 1T and **c** 3R PtX_2 (X = S, Se, and Te). **d** First Brillouin Zone of a hexagonal lattice

Table 1. Lattice Parameters (Å), Formation energy (E_F, eV per formula unit) and band gap (E_G, eV) of bulk 1T and 3R structures of PtX_2 (X = S, Se, Te)

Chalcogen (X)	1T							3R			
	a	Exp.[25]	c	Exp.[25]	E_F	E_G	Other Studies	a	c	E_F	E_G
S	3.591	3.543	4.877	5.039	−5.341	0.25	0.2526	3.554	16.392	−5.323	0.93
Se	3.785	3.728	4.969	5.081	−5.009	−0.78	SM[30,31]	3.734	17.048	−4.98	0.12
Te	4.069	4.026	5.236	5.221	−4.823	−1.17	SM[30,31]	3.986	17.598	−4.778	−1.37

Negative band gap and SM means semimetal

Table 2. Formation energy (E_F, eV per formula unit) and band gap (E_G, eV) of layered 1T and 3R structures of PtX_2 (X = S, Se, Te)

Chalcogen (X)		1		2		3		4		5		6		8		10	
		1T	3R	1T	3R	1T	3R	1T	3R	1T	3R	1T	3R	1T	3R	1T	3R
S	E_F	−5.24	−5.24	−5.29	−5.28	−5.31	−5.29	−5.31	−5.3	−5.32	−5.31	−5.32	−5.31	−5.33	−5.31	−5.33	−5.31
	E_G	1.68	1.68	0.82	1.22	0.67	1.12	0.55	1.06	0.47	1.02	0.41	1	0.34	0.97	0.3	0.95
Se	E_F	−4.88	−4.88	−4.94	−4.94	−4.96	−4.95	−4.98	−4.96	−4.98	−4.96	−4.99	−4.965	−4.99	−4.97	−5	−4.97
	E_G	1.18	1.18	0.21	0.65	−0.08	0.47	−0.29	0.36	−0.43	0.29	−0.53	0.25	−0.64	0.2	−0.71	0.18
Te	E_F	−4.65	−4.65	−4.73	−4.71	−4.76	−4.73	−4.77	−4.75	−4.78	−4.75	−4.79	−4.756	−4.8	−4.76	−4.8	−4.77
	E_G	0.4	0.4	−0.51	−0.34	−0.94	−0.67	−1.06	−0.94	−1.06	−1.07	−1.09	−1.13	−1.17	−1.22	−1.19	−1.28

Negative band gap means semimetal

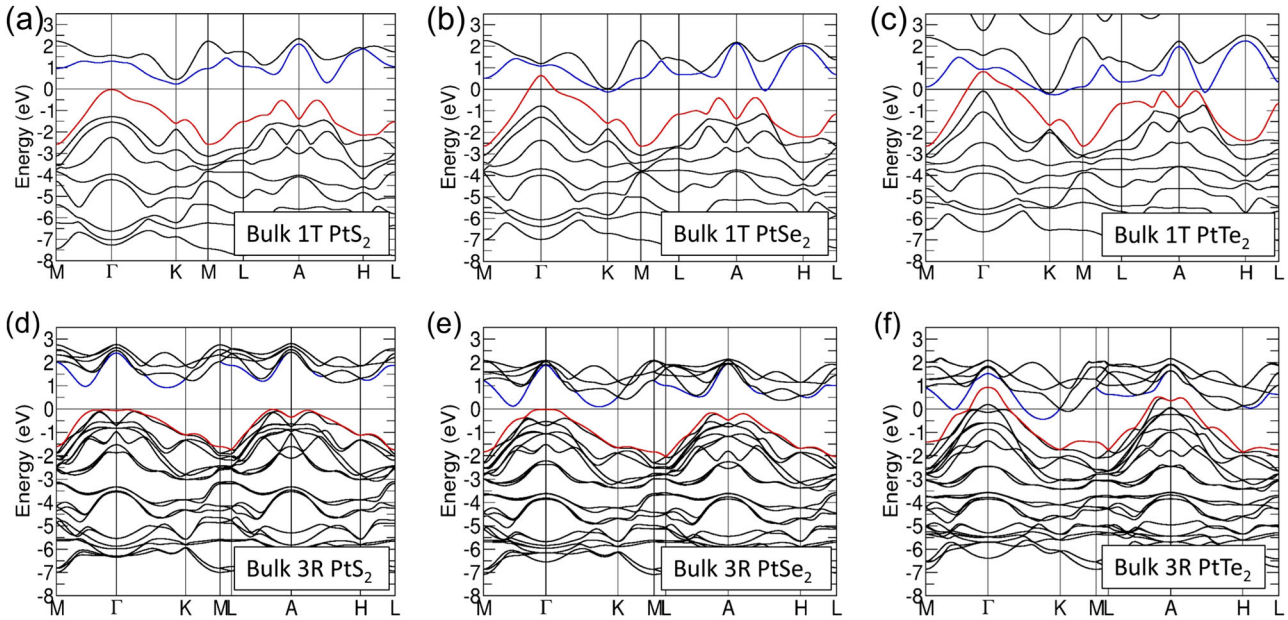

Fig. 2 Band structures of bulk 1T **a**–**c** and 3R **d**–**f** PtX_2 (X = S, Se, and Te)

($E_G = 0.25$ eV), respectively.[25,26] Furthermore, 1T-$PtSe_2$ and 1T-$PtTe_2$ are found to be semi-metallic[30,31] with calculated (experimental[25]) lattice parameters of a = 3.785 Å, c = 4.969 Å and a = 4.069 Å, c = 5.236 Å (a = 3.728 Å, c = 5.081 Å and a = 4.026 Å, c = 5.221 Å), respectively. However, we note that previous studies[30,31] show that bulk 1T-$PtTe_2$ is metallic, in contrast with our results, which we attribute the difference due to the inclusion of spin-orbit coupling (SOC) in our calculations.

Scrutinizing the bulk 1T band structures, we see that the system band gap originates from the top of the VBM at Γ point up to the conduction band at K point for all the chalcogens. With regards to the calculated band structures in 3R, we see that the band of bulk 3R-PtS_2 is still indirect but the gap is now 0.93 eV, which is higher as compared to its 1T counterpart. In addition, bulk 3R-$PtSe_2$ now has an indirect semi-conducting gap of 0.12 eV. Among the three bulk 3R-PtX_2, 3R-$PtTe_2$ remained to be semi-metallic. In Fig. 2, we compare the band structures of bulk 3R with bulk 1T. We see that the system band gap still originates from the VBM at Γ point, but this time, the CBM is now at the middle of Γ and K points. The difference in the electronic band structures of bulk 1T and 3R is due to the breaking of crystal symmetry which affects the high-symmetry points of the BZ.

Next, we explore the thickness dependent properties. The bulk lattice constants (see Table 1) are used to construct the layered structures starting from monolayer up to 10L. Crystal structure relaxations were performed again before determining the formation energies and electronic properties. To understand the effect of the thickness to the electronic structures of layered PtX_2 TMDs, we explored the structural and electronic properties of PtX_2 with respect to increasing the number of layers. We note that for the case of thin film structures, we opted to only show the band structures for 1T-PtX_2 because, to the best of our knowledge, only this structure has been synthesized experimentally.

We now analyze the band structures of each chalcogen starting off with PtS_2. As shown in Fig. 3, the band gap increases as the number of layers decreases, with $E_G = 0.25$ eV in bulk, and $E_G =$ 1.68 eV in monolayer. However, we only observe indirect band gaps as the number of layers decrease,[32] which is unlike MoS_2 and WS_2. But looking closely at the band structures, we see that the VBM moved from Γ point at 10L to the in-between of M and Γ points at the monolayer with the apparent adjustment occurring between the 3L and 4L. We see that at 4L, the VBM is still at the Γ point, but upon decreasing to 3L, the VBM shifted its position. Still, the CBM remains in the middle of M and Γ points.

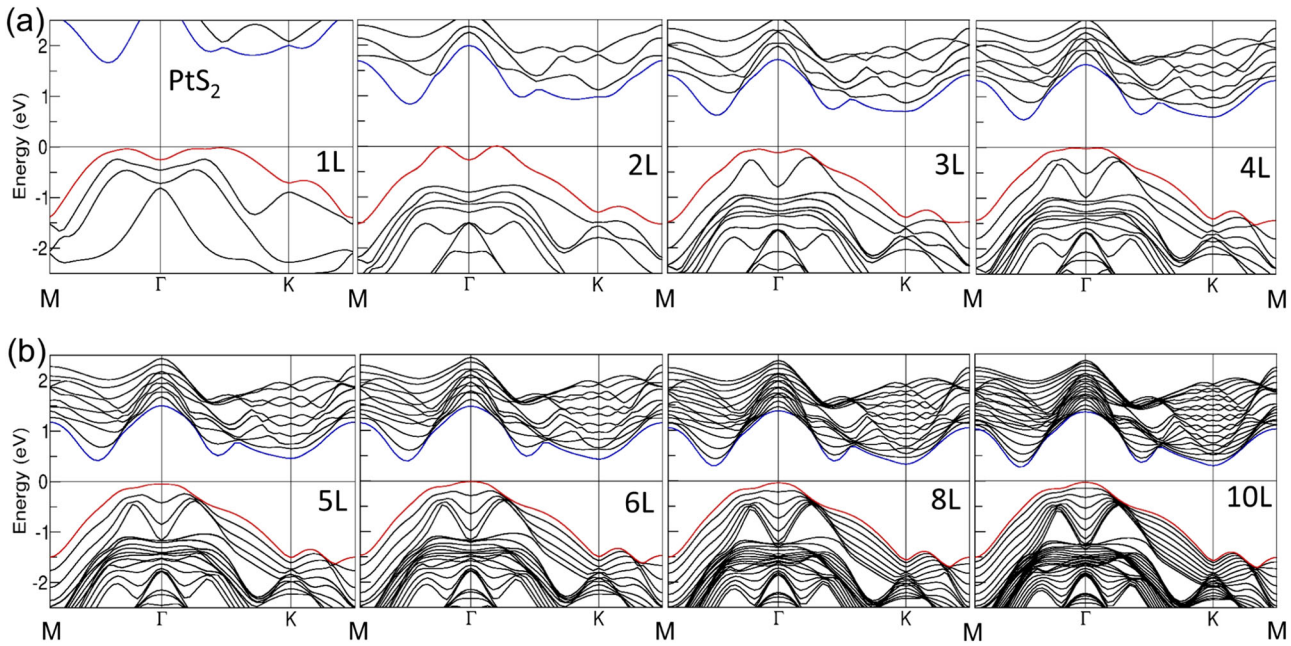

Fig. 3 Band structures of 1T-PtS_2 with varying thickness: **a** 1–4 layers, and **b** 5–10 layers

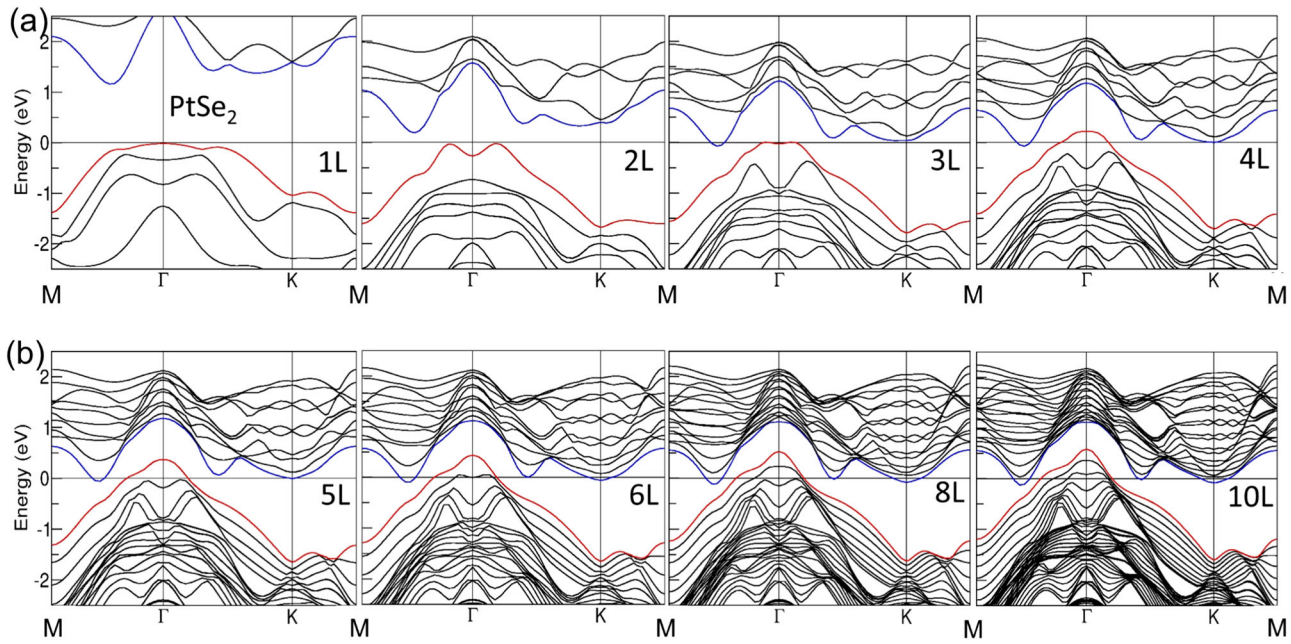

Fig. 4 Band structures of 1T-$PtSe_2$ with varying thickness: **a** 1–4 layers, and **b** 5–10 layers

The evolution of electronic band structure of thin film $PtSe_2$ from monolayer to 10L is shown in Fig. 4. Our results show that 1T-$PtSe_2$ is an indirect band semiconductor only at its mono- and bi-layer with gaps of 1.18 eV and 0.21 eV, respectively, while the structures from 3L to bulk are semi-metallic. Just like in the case of PtS_2, we see that in $PtSe_2$ from 10L to 4L, the VBM is located at Γ point while the CBM is located in-between the M and Γ points. The change also occurs in 3L where both the VBM and CBM, respectively, are located in-between M and Γ points.[29] The difference between PtS_2 and $PtSe_2$ is that the VBM of $PtSe_2$ goes back to the Γ point at monolayer, as opposed to monolayer PtS_2 in which the VBM is still in-between M and Γ points. With this, we observe that there is minimal to no shift of indirect-to-direct band gap as the thickness decrease for the $PtSe_2$ structure.

Among the chalcogens incorporated in this study, Te combined with Pt has the smallest monolayer band gap of 0.40 eV, while the bilayer up to its bulk structure is semi-metallic (see Table 2). Looking closely at band structures of 1T-$PtTe_2$ with varying thickness in Fig. 5, we are still able to observe the decreasing system band gap with increasing number of layers from bilayer to 10 layers. From 3L to 10L, the VBM is located at the Γ point and the CBM is in-between the M and Γ points. However, in bilayer, the VBM and CBM, respectively, are now both located in-between the M and Γ points. Proceeding to the monolayer, we see another

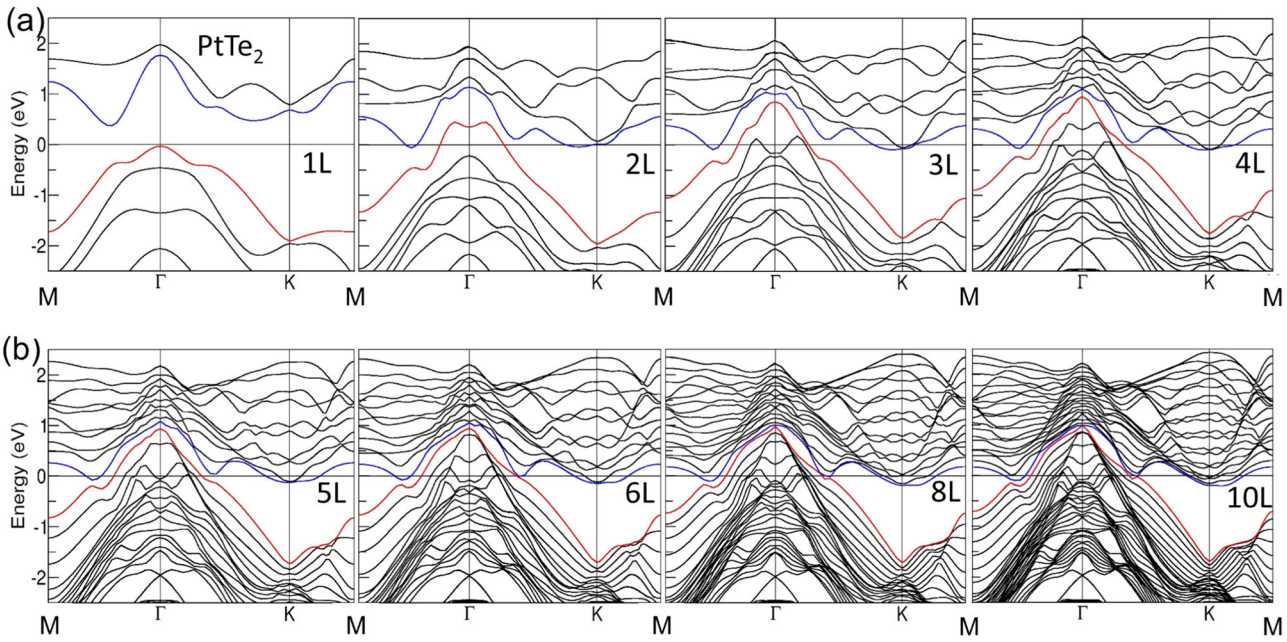

Fig. 5 Band structures of 1T-$PtTe_2$ with varying thickness: **a** 1–4 layers, and **b** 5–10 layers

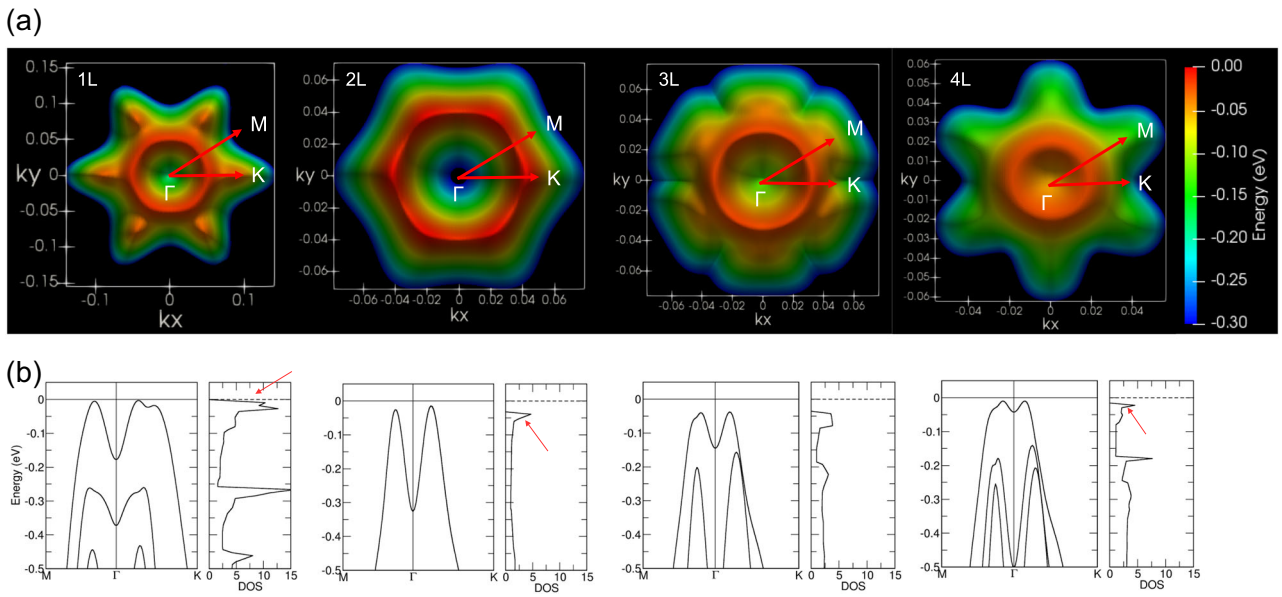

Fig. 6 **a** is the band energy contours of the highest valence band around Γ point of PtS_2 from monolayer up to 4L, **b** is the corresponding band structures with DOS

transition of the VBM going back to Γ point, but this time, the structure is now a semiconductor with an indirect band gap of 0.40 eV. Although PtX_2 are an indirect bandgap semiconductors, a transition from indirect to direct bandgap can be tuned by strain.[14,33,34]

In all 1T-PtX_2 (X = S, Se, and Te) TMDs investigated in this study, we were able to observe an increasing system band gap with decreasing number of layers from bulk down to monolayer structures. However, unlike other TMDs like MX_2 (M = Mo and W; X = S, Se, and Te) which are direct bandgap semiconductors at monolayer,[2] we were not able to observe a shift from indirect-to-direct band gap as the number layers decrease from bulk to monolayer structures. A possible reason for this uniqueness is due to the difference in crystal structure – MX_2 has the 2H structure while PtX_2 has the 1T structure. This dissimilarity in crystal symmetries greatly contributes on how the electronic properties will behave. Nevertheless, we are still able to observe the inverse relationship between the band gap and the number of layers. This phenomenon is governed by factors such as quantum confinement effect[18] and interlayer interaction through van der Waals interaction.[43]

Moreover, upon further inspection of the band structures, we were able to observe a flat band dispersion near the Fermi level of unstrained (0.0%) 4L 1T-PtS_2 as shown in Fig. 6b. When a band in a dispersion curve is flat, this indicates that a lot of allowed states occupy almost the same energy levels. This results to high or diverging density of states (DOS) which is the characteristic feature of vHs.[39,44] Moreover, previous studies[45,46] on graphene and phosphorene have shown that by inducing strain, one can tune the presence and/or location of the vHs relative to the Fermi

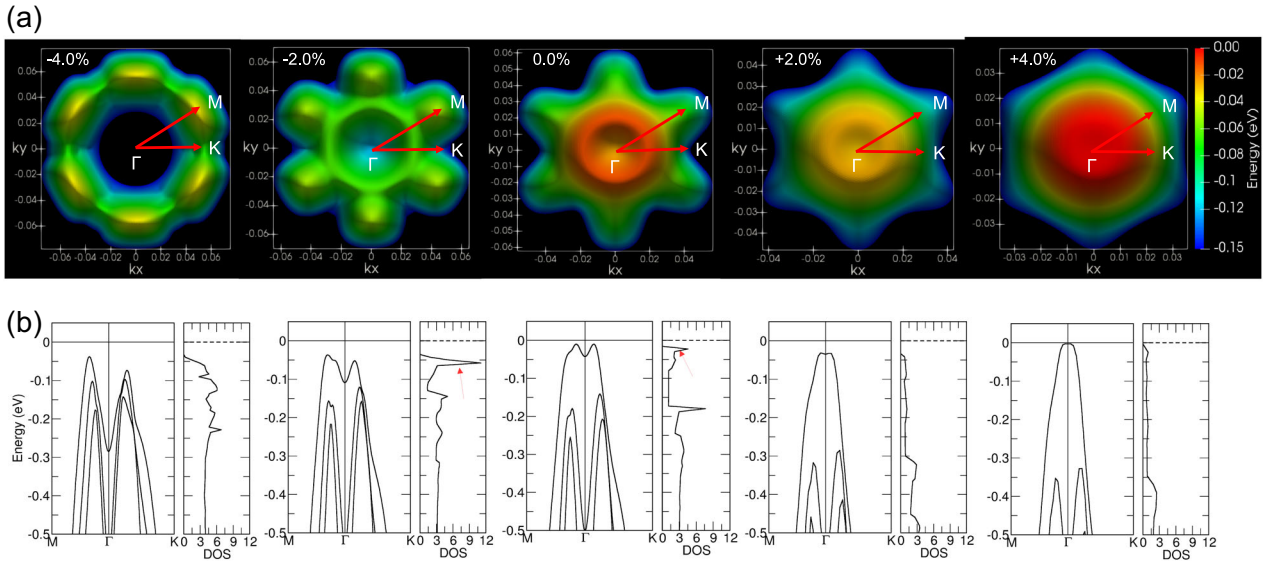

Fig. 7 **a** is the band energy contours of the highest valence band around Γ point of 4L—PtS_2 with varying strain, **b** is the corresponding band structures with DOS

level, which is indicated by saddle points, resulting to high density of states. With this in mind, we plotted the band energy contour and band structure with DOS for monolayer to 4L PtS_2 (Fig. 6). We immediately see the presence of vHs near the Fermi level in monolayer along Γ-K (Fig. 6a), as confirmed in DOS indicated by the red arrow (Fig. 6b). We also see the possible vHs in bilayer and 4L along Γ-M (highlighted by the red arrows).

Since the vHs in 4L is closer to the Fermi level than bilayer, we applied biaxial strain (from −4 to 4%) to the former and plotted the band energy contours (Fig. 7a) and band structures with DOS (Fig. 7b) to investigate the effect of strain. We found a substantial enhancement of vHs in the −2.0% strain with respect to the unstrained case, as indicated by the higher DOS intensity in the former. Our results show that, indeed, the vHs can be tuned by controlling the thickness and straining the material.

In conclusion, because of their unique electronic properties which could be tuned just by manipulating the thickness or inducing strain, the interest for 2D TMDs has been on the rise for the past few years since the discovery of graphene. Furthermore, the discovery of an efficient way to synthesize few-layer $PtSe_2$ rekindled the fascination to Pt-based TMDs regarding their possible properties and applications. In this study, using first-principles calculations, we examined the layer dependence of the electronic properties of PtX_2 TMDs. Moreover, we found a possible metastable 3R structure with comparable formation energy to the 1T structure, the most energetically favorable structure of PtX_2. Our results show that 1T-PtS_2 is an indirect semiconductor with the band gap decreasing from 1.68 eV (monolayer) to 0.25 eV (bulk). Although 1T-$PtSe_2$ is only semiconducting in bilayer and monolayer with band gap equal to 0.21 and 1.18 eV, respectively, we were able to observe a similar trend that its system band gap decreases as the number of layer number increases from monolayer to 10L. For 1T-$PtTe_2$, we found that its monolayer has the smallest band gap equal to 0.40 eV as compared to the other monolayers, and it is only semiconducting in the monolayer structure. Nonetheless, we were still able to observe the decrease in band gap as the number of layers increase from bilayer up to 10L. Overall, we see that Pt-based TMDs exhibits an inverse relationship between its band gap and its thickness which is due to the interplay between quantum confinement effect and interlayer interactions. Additionally, we were able to find diverging density of states in some layered PtS_2, indicating the presence of vHs. Moreover, we show that strain can tune the presence of vHs near the Fermi level. Finally, our results definitely show that the electronic structures of Pt-based TMDs possess high tunability and sensitivity to change in its thickness which could be utilized for future potential applications.

METHODS

We performed our first-principles calculations within the density functional theory framework[47] using projector-augmented wave[48,49] wave functions with energy cut-off energy of 400 eV. We used optB88-vdW functional[50–53] for van der Waals correction in addition to GGA-PW91[54–56] pseudopotential as implemented in the Vienna Ab-Initio Simulation Package (VASP).[57–60] All crystal structure relaxations were conducted until the residual force acting on each atom is less than 0.01 eV/A. The self-consistent convergence criterion for electronic structures was set to 10^{-6} eV. We sampled the first brillouin zone (BZ) using Γ-centered Monkhorst-Pack[61] grids of 18 × 18 × 13, 18 × 18 × 4, and 18 × 18 × 1 for bulk 1T, 3R, and thin film structures, respectively. To simulate finite-layer structures, we added a vacuum of 25 Å above the topmost layer to eliminate the interactions due to periodic boundary conditions. All calculations are done with the inclusion of SOC. We tested several pseudopotentials combined with different vdW correction functionals, in which we found that GGA-PW91[54–56] combined with optB88-vdW[50–53] yielded the most accurate band gap results without sacrificing the correctness of the lattice parameters relative to the experimental result.[25] For the strain calculations, we implemented compressive (-) and tensile (+) strain. In applying the strain, we changed the lattice constant then did another relaxation calculation while only allowing the atomic positions to change and fixing the lattice constant. Moreover, we used 300 × 300 × 1 kpoint mesh to get an accurate energy contour plot.

DATA AVAILABILITY

The authors declare that all relevant data are available from the authors. The details of the coordinates of all the calculated systems, including the lattice vectors, are uploaded in a permanent repository with https://doi.org/10.5281/zenodo.1975488.[62]

ACKNOWLEDGEMENTS

FCC acknowledges support from the National Center for Theoretical Sciences and the Ministry of Science and Technology of Taiwan under Grants No. MOST-104-2112-M-110-002-MY3 and MOST 107-2628-M-110-001-MY3. He is also grateful to the National Cen0ter for High-Performance Computing for computer time and facilities. SMH is supported from the Ministry of Science and Technology (MoST) in Taiwan under Grant No. 105-2112-M-110-014-MY3.

AUTHOR CONTRIBUTIONS

F.C.C. and H.L. conceived and initiated the study. R.A.V., C.P.C., and Z.Q.H., performed first principles calculations. R.A.V., S.M.H., F.C.C., and H.L. performed the analysis regarding the vHs. R.A.V., C.P.C., Z.Q.H., S.M.H., A.A.B., M.A., H.L., and F.C.C. performed the detailed analysis and contributed to discussions and wrote the manuscript. All authors reviewed the manuscript.

ADDITIONAL INFORMATION

Competing interests: The authors declare no competing interests.

Publisher's note: Springer Nature remains neutral with regard to jurisdictional claims in published maps and institutional affiliations.

REFERENCES

1. Golden, J. et al. Rhenium variations in molybdenite (MoS_2): Evidence for progressive subsurface oxidation. *Earth Planet. Sci. Lett.* **366**, 1–5 (2013).
2. Kolobov, A. V. & Tominaga, J. *Two-dimensional Transition-metal Dichalcogenides*, Vol. 239 (Springer International Publishing AG, Switzerland, 2016).
3. Dickinson, R. G. & Pauling, L. The crystal structure of molybdenite. *J. Am. Chem. Soc.* **45**, 1466–1471 (1923).
4. Frindt, R. F. Single crystals of MoS_2 several molecular layers thick. *J. Appl. Phys.* **37**, 1928–1929 (1966).
5. Joensen, P., Frindt, R. F. & Morrison, S. R. Single-layer MoS_2. *Mater. Res. Bull.* **21**, 457–461 (1986).
6. Wilson, J. A. & Yoffe, A. D. The transition metal dichalcogenides discussion and interpretation of the observed optical, electrical and structural properties. *Adv. Phys.* **18**, 193–335 (1969).
7. Novoselov, K. S. et al. Electric field effect in atomically thin carbon films. *Science.* **306**, 666–669 (2004).
8. Ramakrishna Matte, H. S. S. et al. MoS2 and WS2 analogues of graphene. Angew. Chem. Int. **49**, 4059–4062 (2010).
9. Roldán, R. et al. Electronic properties of single-layer and multilayer transition metal dichalcogenides MX_2 (M = Mo, W and X = S, Se). *Ann. Phys.* **526**, 347–357 (2014).
10. Ellis, J. K., Lucero, M. J. & Scuseria, G. E. The indirect to direct band gap transition in multilayered MoS_2 as predicted by screened hybrid density functional theory. *Appl. Phys. Lett.* **99**, 261908 (2011).
11. Conley, H. J. et al. Bandgap engineering of strained monolayer and bilayer MoS_2. *Nano Lett.* **13**, 3626–3630 (2013).
12. He, X. et al. Strain engineering in monolayer WS_2, MoS_2, and the WS_2/MoS_2 heterostructure. *Appl. Phys. Lett.* **109**, 173105 (2016).
13. Shen, T., Penumatcha, A. V. & Appenzeller, J. Strain engineering for transition metal dichalcogenides based field effect transistors. *ACS Nano* **10**, 4712–4718 (2016).
14. Guo, S. & Wang, Y. Small compressive strain-induced semiconductor—metal transition and tensile strain-enhanced thermoelectric properties in monolayer $PtTe_2$. *Semicond. Sci. Technol.* **32**, 7 (2017). pp.
15. Zhang, Y. et al. Direct observation of the transition from indirect to direct bandgap in atomically thin epitaxial $MoSe_2$. *Nat. Nanotechnol.* **9**, 111–115 (2014).
16. Jin, W. et al. Direct measurement of the thickness-dependent electronic band structure of MoS_2 using angle-resolved photoemission spectroscopy. *Phys. Rev. Lett.* **111**, 106801 (2013).
17. Zeng, H. et al. Optical signature of symmetry variations and spin-valley coupling in atomically thin tungsten dichalcogenides. *Sci. Rep.* **3**, 2–6 (2013).
18. Kuc, A., Zibouche, N. & Heine, T. How does quantum confinement influence the electronic structure of transition metal sulfides TmS_2. *Phys. Rev. B* **83**, 1–4 (2011).
19. Wang, Y. et al. Monolayer $PtSe_2$, a new semiconducting transition-metal-dichalcogenide, epitaxially grown by direct selenization of Pt. *Nano Lett.* **15**, 4013–4018 (2015).
20. O'Brien, M. et al. Raman characterization of platinum diselenide thin films. *2D Mater.* **3**, 021004 (2016).
21. Ciarrocchi, A., Avsar, A., Ovchinnikov, D. & Kis, A. Thickness-modulated metal-to-semiconductor transformation in a transition metal dichalcogenide. *Nat. Commun.* **9**, 1–6 (2018).
22. Yu, X. et al. Atomically thin noble metal dichalcogenide: A broadband mid-infrared semiconductor. *Nat. Commun.* **9**, 1–9 (2018).
23. Zhao, Y. et al. High-Electron-Mobility and Air-Stable 2D Layered $PtSe_2$ FETs. *Adv. Mater.* **29**, 1–10 (2016).
24. Chia, X. et al. Layered platinum dichalcogenides (PtS_2, $PtSe_2$, and $PtTe_2$) electrocatalysis: monotonic dependence on the chalcogen size. *Adv. Funct. Mater.* **26**, 4306–4318 (2016).
25. Furuseth, S. et al. Redetermined crystal structures of $NiTe_2$, $PdTe_2$, PtS_2, $PtSe_2$, and $PtTe_2$. *Acta Chem. Scand.* **19**, 257–258 (1965).
26. Zhao, Y. et al. Extraordinarily strong interlayer interaction in 2D layered PtS_2. *Adv. Mater.* **28**, 2399–2407 (2016).
27. Su, T. Y. et al. Phase-engineered $PtSe_2$-layered films by a plasma-assisted selenization process toward all $PtSe_2$-based field effect transistor to highly sensitive, flexible, and wide-spectrum photoresponse photodetectors. *Small* **14**, 1–10 (2018).
28. Sajjad, M., Singh, N. & Schwingenschlögl, U. Strongly bound excitons in monolayer PtS_2 and $PtSe_2$. *Appl. Phys. Lett.* **112**, 043101 (2018).
29. Kandemir, A. et al. Structural, electronic and phononic properties of PtSe2: From monolayer to bulk. *Semicond. Sci. Technol.* **33**, 085002 (2018).
30. Guo, G. Y. & Liang, W. Y. The electronic structures of platinum dichalcogenides: PtS_2, $PtSe_2$ and $PtTe_2$. *J. Phys. C. Solid State Phys.* **19**, 995–1008 (1986).
31. Dai, D. et al. Trends in the structure and bonding in the layered platinum dioxide and dichalcogenides PtQ_2(Q = O, S, Se, Te). *J. Solid State Chem.* **173**, 114–121 (2003).
32. Mirõ, P., Ghorbani-Asl, M. & Heine, T. Two dimensional materials beyond MoS2: noble-transition-metal dichalcogenides. Angew. Chem. Int. **5**3, 3015–3018 (2014).
33. Liu, G., Gan, Y., Quhe, R. & Lu, P. Strain dependent electronic and optical properties of PtS_2 monolayer. *Chem. Phys. Lett.* **709**, 65–70 (2018).
34. Li, P., Li, L. & Zeng, X. C. Tuning the electronic properties of monolayer and bilayer PtS_e2: Via strain engineering. *J. Mater. Chem. C.* **4**, 3106–3112 (2016).
35. Zhang, W., Qin, J., Huang, Z. & Zhang, W. The mechanism of layer number and strain dependent bandgap of 2D crystal $PtSe_2$. *J. Appl. Phys.* **122**, 205701 (2017).
36. Van Hove, L. Correlations in space and time and born approximation scattering in systems of interacting particles. *Phys. Rev.* **95**, 249–262 (1954).
37. Kohn, W. & Luttinger, J. M. New mechanism for superconductivity. *Phys. Rev. Lett.* **15**, 524–526 (1965).
38. Hirsch, J. E. & Scalapino, D. J. Enhanced superconductivity in quasi two-dimensional systems. *Phys. Rev. Lett.* **56**, 2732–2735 (1986).
39. Honerkamp, C. & Salmhofer, M. Magnetic and superconducting instabilities of the hubbard model at the van hove filling. *Phys. Rev. Lett.* **8**7, 187004 (2001).
40. Fleck, M., Oles, A. M. & Hedin, L. Magnetic phases near the Van Hove singularity in s and d-band Hubbard model. *Phys. Rev. B* **56**, 8 (1999).
41. Hlubina, R., Sorella, S. & Guinea, F. Ferromagnetism in the two dimensional t−t′ hubbard model at the van hove density. *Phys. Rev. Lett.* **78**, 1343–1346 (1997).
42. Lin, H. Q. & Hirsch, J. E. Two-dimensional Hubbard model with nearest- and next-nearest-neighbor hopping. *Phys. Rev. B* **35**, 3359–3368 (1987).
43. Das, R., Pandey, S. K. & Mahadevan, P. Layer dependent electronic structure changes in transition metal dichalcogenides—the role of geometric confinement. arXiv: https://arxiv.org/abs/1702.04535. 1–17 (2017).
44. Noda, K., Inaba, K. & Yamashita, M. Magnetism in the three-dimensional layered Lieb lattice: enhanced transition temperature via flat-band and Van Hove singularities. *Phys. Rev. A.* **91**, 1–7 (2015).
45. Ziletti, A., Huang, S. M., Coker, D. F. & Lin, H. Van Hove singularity and ferromagnetic instability in phosphorene. *Phys. Rev. B.* **92**, 1–11 (2015).
46. Chu, Z. D., He, W. Y. & He, L. Coexistence of van Hove singularities and superlattice Dirac points in a slightly twisted graphene bilayer. *Phys. Rev. B.* **87**, 2–9 (2013).
47. Hohenberg, P. & Kohn, W. Inhomogeneous electron gas. *Phys. Rev.* **136**, B864–B871 (1964).
48. Blöchl, P. E. Projector augmented-wave method. *Phys. Rev. B* **50**, 17953–17979 (1994).
49. Kresse, G. & Joubert, D. From ultrasoft pseudopotentials to the projector augmented-wave method. *Phys. Rev. B* **59**, 1758–1775 (1999).
50. Dion, M., Rydberg, H., Schröder, E., Langreth, D. C. & Lundqvist, B. I. Van der Waals density functional for general geometries. *Phys. Rev. Lett.* **92**, 22–25 (2004).
51. Thonhauser, T. et al. Van der Waals density functional: Self-consistent potential and the nature of the van der Waals bond. *Phys. Rev. B.* **76**, 1–11 (2007).
52. Klimeš, J., Bowler, D. R. & Michaelides, A. Chemical accuracy for the van der Waals density functional. *J. Phys. Condens. Matter* **22**, 022201 (2010).
53. Klimeš, J., Bowler, D. R. & Michaelides, A. Van der Waals density functionals applied to solids. *Phys. Rev. B.* **83**, 1–13 (2011).
54. Perdew, J. P. & Wang, Y. Accurate and simple analytic representation of the electron-gas correlation energy. *Phys. Rev. B* **45**, 244–249 (1992).
55. Perdew, J. et al. Atoms, molecules, solids, and surfaces: Applications of the generalized gradient approximation for exchange and correlation. *Phys. Rev. B* **46**, 6671–6687 (1992).
56. Perdew, J. P. et al. Erratum: atoms, molecules, solids, and surfaces: applications of the generalized gradient approximation for exchange and correlation. *Phys. Rev. B* **48**, 4978–4978 (1993).
57. Kresse, G. & Hafner, J. Ab initio molecular dynamics for liquid metals. *Phys. Rev. B* **47**, 558–561 (1993).

58. Kresse, G. & Hafner, J. Ab initio molecular-dynamics simulation of the liquid-metal–amorphous-semiconductor transition in germanium. *Phys. Rev. B* **49**, 14251–14269 (1994).
59. Kresse, G. & Furthmüller, J. Efficient iterative schemes for ab initio total-energy calculations using a plane-wave basis set. *Phys. Rev. B* **54**, 11169–11186 (1996).
60. Kresse, G. & Furthmüller, J. Efficiency of ab-initio total energy calculations for metals and semiconductors using a plane-wave basis set. *Comput. Mater. Sci.* **6**, 15–50 (1996).
61. Monkhorst, H. J. & Pack, J. D. Special points for Brillouin-zone integrations. *Phys. Rev. B* **13**, 5188–5192 (1976).
62. Villaos, R. A. et. al. Thickness dependent electronic properties of Pt dichalcogenides—PtX_2 (X = S, Se, and Te). (2018). https://doi.org/10.5281/zenodo.1975488.